of a momentum-dependent pole in the spin susceptibility due to antiferromagnetic interactions (*20*). This picture also accounts for the rapidly diminishing intensity of the magnetic peaks away from (π, π), as collective modes commonly lose oscillator strength upon approaching the continuum. Models based on dynamical nesting induced by a modification of the band dispersions (*21–23*) may also be consistent with our data. The models favored by our experimental results on near optimally doped $YBa_2Cu_3O_{6+x}$ are based on an interplay between band dispersions, Coulomb interactions, and the *d*-wave gap function in a 2D correlated electronic state.

References and Notes

1. J. M. Tranquada *et al.*, *Nature* **375**, 561 (1995).
2. V. J. Emery and S. A. Kivelson, *Physica C* **209**, 597 (1993).
3. T. E. Mason *et al.*, *Phys. Rev. Lett.* **68**, 1414 (1992).
4. T. R. Thurston *et al.*, *Phys. Rev. B* **46**, 9128 (1992).
5. S. Petit *et al.*, *Physica B* **234–236**, 800 (1997).
6. K. Yamada *et al.*, *Phys. Rev. B* **57**, 6165 (1998).
7. J. Rossat-Mignod *et al.*, *Physica C* **185–189**, 86 (1991).
8. H. A. Mook *et al.*, *Phys. Rev. Lett.* **70**, 3490 (1993).
9. H. F. Fong *et al.*, *Phys. Rev. Lett.* **75**, 316 (1995).
10. P. Bourges, L. P. Regnault, Y. Sidis, C. Vettier, *Phys. Rev. B* **53**, 876 (1996).
11. H. F. Fong, B. Keimer, D. Reznik, D. M. Milius, I. A. Aksay, *Phys. Rev. B* **54**, 6708 (1996).
12. P. Bourges, in *The Gap Symmetry and Fluctuations in High Temperature Superconductors*, J. Bok *et al.*, Eds. (Plenum, New York, 1998), pp. 349–371 (e-Print available at http://xxx.lanl.gov/abs/cond-mat/9901333).
13. L. P. Regnault, P. Bourges, P. Burlet, in *Neutron Scattering in Layered Copper-Oxide Superconductors*, A. Furrer, Ed. (Kluwer, Amsterdam, 1998), pp. 85–134.
14. H. F. Fong, B. Keimer, F. Dogan, I. A. Aksay, *Phys. Rev. Lett.* **78**, 713 (1997).
15. P. Bourges *et al.*, *Europhys. Lett.* **38**, 313 (1997).
16. P. Dai *et al.*, *Phys. Rev. Lett.* **80**, 1738 (1998).
17. H. A. Mook *et al.*, *Nature* **395**, 580 (1998).
18. M. Arai *et al.*, *Phys. Rev. Lett.* **83**, 608 (1999).
19. D. van der Marel, *Phys. Rev. B* **51**, 1147 (1995).
20. F. Onufrieva and P. Pfeuty, e-Print available at http://xxx.lanl.gov/abs/cond-mat/9903097.
21. J. Brinckmann and P. Lee, *Phys. Rev. Lett.* **82**, 2915 (1999).
22. Y.-J. Kao, Q. Si, K. Levin, e-Print available at http://xxx.lanl.gov/abs/cond-mat/9908302.
23. K.-K. Voo and W. C. Wu, e-Print available at http://xxx.lanl.gov/abs/cond-mat/9911321.
24. H. F. Fong *et al.*, *Phys. Rev. B.*, in press (e-Print available at http://xxx.lanl.gov/abs/cond-mat/9910041).
25. On IN8, a Cu(111) monochromator and a pyrolytic graphite PG(002) analyzer, set at a fixed final energy of 35 meV, were used. On 2T, PG(002) was employed as both monochromator and analyzer with a 14.7-meV fixed final energy. In both experiments, a PG filter was inserted into the scattered beam to remove higher order contamination. The sample was wrapped in aluminum foil and attached to the cold finger of a closed-cycle helium refrigerator.
26. For simplicity, we describe the data with an isotropic dispersion relation (α independent of *q*). A slight anisotropy of α between the (100) and (110) directions, with an associated intensity modulation, would reproduce the detailed momentum dependence reported in (*17*).
27. Above 45 meV, the magnetic peaks are characterized by a broader response (*18, 24*) reminiscent of the spin waves of the undoped compound [see P. Bourges *et al.*, *Phys. Rev. B* **56**, R11439 (1997)].
28. A. V. Balatsky and P. Bourges, *Phys. Rev. Lett.* **82**, 5337 (1999).
29. P. Bourges *et al.*, in *High Temperature Superconductivity*, S. E. Barnes *et al.*, Eds. (American Institute of Physics, Amsterdam, 1999), pp. 207–212 (e-Print available at http://xxx.lanl.gov/abs/cond-mat/9902067).
30. G. Aeppli, T. E. Mason, S. M. Hayden, H. A. Mook, J. Kulda, *Science* **278**, 1432 (1997).

31. We thank P. Baroni for his help during the experiment at Laboratoire Léon Brillouin and G. Aeppli, B. Hennion, G. Khaliullin, F. Onufrieva, and P. Pfeuty for stimulating discussions. The work at Princeton University was supported by the Materials Research Science and Engineering Centers program of the NSF under DMR-9809483.

17 January 2000; accepted 29 March 2000

Propagation of Seismic Ground Motion in the Kanto Basin, Japan

Kazuki Koketsu* and Masayuki Kikuchi

The pattern of ground motion for a magnitude 5.7 earthquake near Tokyo was captured by 384 strong ground motion instruments across the Kanto sedimentary basin and its surroundings. The records allow the visualization of the propagation of long-period ground motion in the basin and show the refraction of surface waves at the basin edge. The refracted wave does not travel directly from the earthquake epicenter, but traverses the basin obliquely to the edge. The surface wave inside the basin propagates more slowly than that outside such that the wavefronts separate from each other, and the refracted wave heals the discrepancy in the speed of advance of the wavefronts inside and outside the basin. The refracted arrival is dominant near the edge of the Kanto basin.

Seismic ground motion should be distorted and amplified by its propagation through sedimentary basins (*1*). However, observations of the effects of such propagation are limited because there have not been dense networks of strong ground motion seismometers that extend beyond the basins. Following the destructive earthquake in Kobe in 1995, the Japanese government realized that lack of prompt information on ground motion distribution was fatal to rescue and recovery actions immediately after a large earthquake. As a result, a dense network of strong ground motion seismometers and seismic intensity meters was installed across Japan (*2*, *3*). The intensity meters observe ground motion like a strong ground motion seismometer and automatically calculate the seismic intensity defined by the Japan Meteorological Agency.

Tokyo is situated in a large-scale sedimentary basin called the Kanto basin with an area of about 17,000 km^2. More than 600 strong ground motion instruments have been installed in the basin and its surroundings (Fig. 1). A magnitude 5.7 earthquake at a depth of 2.8 km on 3 May 1998 off the Izu peninsula (to the southwest of Tokyo) was observed by 384 sensors. This kind of shallow undersea earthquake often generates long-period surface Love waves, and these waves are clearly seen in the Kanto basin with periods of about 8 s (*4*). The large number of observations enabled us to visualize the propagation of the ground motion associated with these Love waves. To emphasize these arrivals, we first converted the accelerograms recorded by the instruments to velocity seismograms and applied a low-pass filter with a corner period of 5 s (Fig. 2A). Then we plotted the trajectories of ground motion in the horizontal plane for consecutive 10 s intervals after source initiation (Fig. 2, A to D) overlaid on an index map. These plots provide a clear indication of the progression of Love wave energy across the set of sensors.

The density of the instrument distribution, especially in the western mountain range, is not sufficient to allow interpolation of the data to produce a spatially continuous distribution of the ground motion. However, the Love wave generates ground motion parallel to its wavefront (perpendicular to its propagation path), so the trajectory of ground motion at each observation point can help us identify the wavefront and path. We normalized each particle trajectory to the maximum amplitude for the recording duration to make visible small ground motions in the mountain range (Fig. 2).

We identified wavefronts by noting abrupt changes in the amplitude and trajectory of ground motion. Small, near-circular motion before the arrival of the Love wave represents long-period components of the S body waves and is noticeable in the northeastern part of Fig. 2D due to the effects of the local geology. The pattern of particle motion in the center of the basin is contaminated by

Earthquake Research Institute, University of Tokyo, Tokyo 113-0032, Japan.

*To whom correspondence should be addressed. E-mail: inquiry@taro.eri.u-tokyo.ac.jp

the long tail of the S-wave train and the complexity of surface wave propagation in the shallow sedimentary layers, leading to more elliptical particle trajectories.

The wavefront to the west through the mountain ranges travels with a speed of 3.5 to 4 km/s, whereas that in the center of the basin propagates as slow as 1.0 km/s (Fig. 2). The difference between the propagation velocities causes a discontinuity between the wavefronts, and a part of the Love wave in the mountain range is transformed into refracted surface waves in order to heal the wavefront discontinuity (Fig. 2, B and C). The process is analogous to the generation of a head wave at an interface separating wavefronts of transmitted and reflected body waves. The refracted surface wave is dominant toward the edge of the basin and appears to propagate from the boundary between the basin and mountain range rather than from the epicenter.

Numerical simulations of seismic ground motion (*5–7*) and localized array analyses (*4*, *8*) suggest the presence of such surface waves

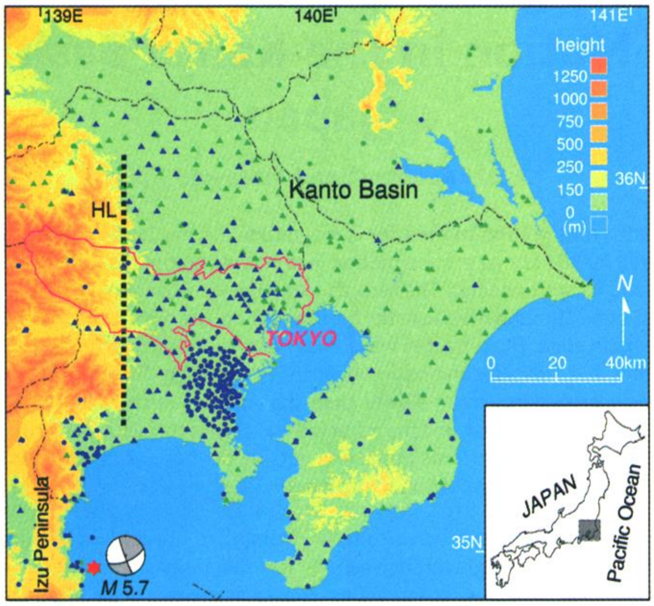

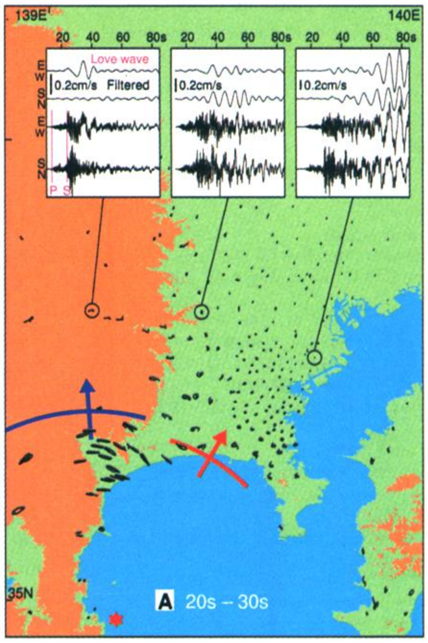

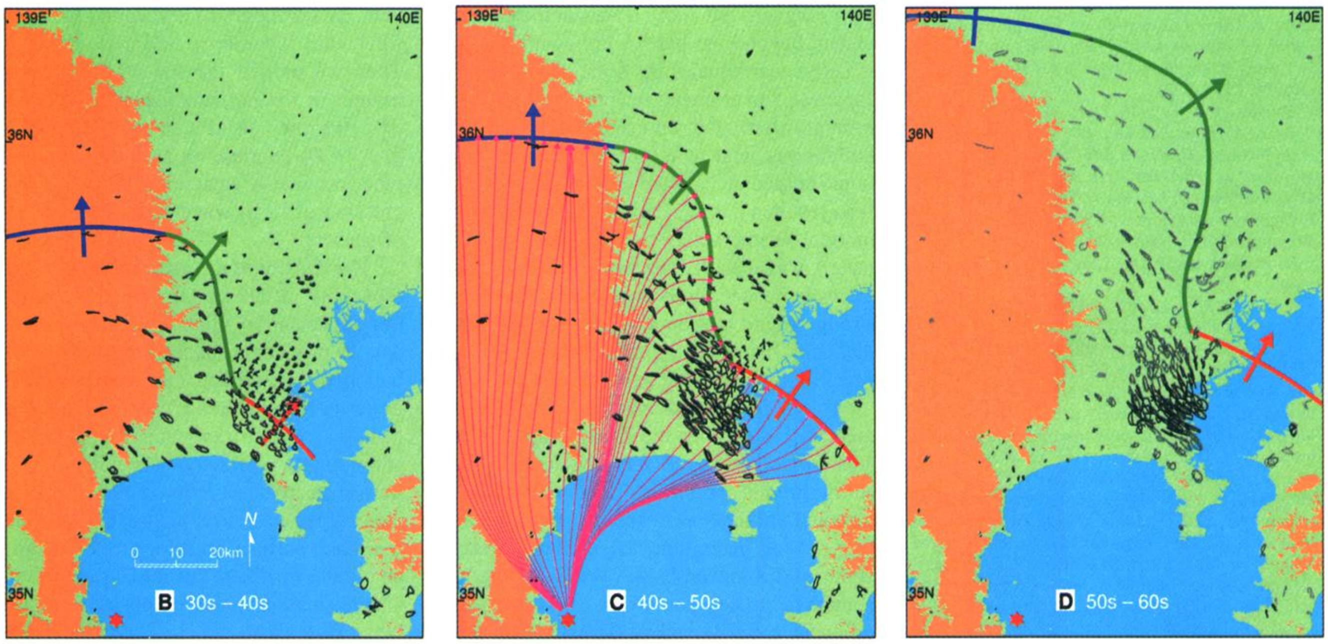

Fig. 1 (upper left). Distribution of strong ground motion seismometers (blue and green circles) and seismic intensity meters (blue and green triangles) in the Kanto basin; 384 of these instruments (blue symbols) observed a magnitude 5.7 earthquake on 3 May 1998 (red star with focal mechanism) to the southwest of Tokyo (surrounded by fuschia lines). The western edge of the basin, termed the Hachioji line (HL, black vertical dashed line) almost coincides with an altitude contour of 150 m. **Fig. 2** (begins upper right). Horizontal ground velocity motion trajectories (black ellipses) for 10 s intervals starting at (**A**) 20 s, (**B**) 30 s, (**C**) 40 s, and (**D**) 50 s after the earthquake. The ground motions have been low-pass filtered with a corner period of 5 s as shown in the insets in (A) and normalized to the maximum amplitudes for the recording duration. The trajectories are overlaid on an index map wherein the light green represents the basin with elevations lower than 150 m and orange represents the surrounding mountain ranges. The red and blue arcs are the wavefronts traveling inside and outside the basin, respectively, and the green curve indicates the refracted Love wave. The calculated ray paths for Love waves that match these wavefronts are shown in (C) by magenta arrows and are derived from the 3D structural model (*9*, *10*) for the Kanto basin. To indicate the effects of site amplification, we plotted the ellipses in (D) in a gray scale with darker lines corresponding to higher amplitude.

that do not come directly from the epicenter. The generation process of such a surface wave is reproduced here from the real records, and its physical mechanism is interpreted as refraction to compensate for a wavefront discontinuity.

To confirm the interpretation of the ground motion pattern, we performed ray tracing for Love waves in models of the structure in the Kanto basin (*9*, *10*). The S-wave velocities in the basement and sedimentary layers are estimated from P-wave data because they are not well constrained from the previous studies. The model for ray tracing uses the local-mode approximation (*11*), employing a 100×100 grid with a spacing of 2.00 km (E/W) and 1.75 km (N/S). A horizontally layered structure is retrieved from the three-dimensional (3D) structural model at each point, and the phase velocity of the fundamental mode of the Love wave is then calculated for each grid point at a period of 8 s. We carried out ray tracing in this phase velocity distribution with the shooting method (*12*). The calculated rays were traced to 40 s after the origin time of the earthquake (Fig. 2C). Because rays are defined as normal to a wavefront, the tips of the rays indicate the theoretical wavefronts at 40 s, which agree well with the observed wavefronts.

References and Notes

1. T. H. Heaton, J. F. Hall, D. J. Wald, M. W. Halling, *Science* **267**, 206 (1995).
2. S. Kinoshita, *Seismol. Res. Lett.* **69**, 309 (1998).
3. Japan Meteorological Agency, *On Seismic Intensity* (Gyosei, Tokyo, 1996).
4. S. Zama, *Proceedings of the 10th World Conference on Engineering*, 19 to 24 July 1992, Madrid, Spain (A. A. Balkema, Rotterdam, Netherlands, 1992). Surface waves induced from S body waves at a basin edge are known as another kind of seismic phenomenon related to a sedimentary basin [E. D. Field, *Bull. Seismol. Soc. Am.* **86**, 991 (1996)]. Such waves are expected to have been generated for this earthquake, but would be buried in the well-developed Love wave coming from the source region.
5. K. Yomogida and J. T. Etgen, *Bull. Seismol. Soc. Am.* **83**, 1325 (1993).
6. K. B. Olsen, R. J. Archuleta, J. R. Matarese, *Science* **270**, 1628 (1995).
7. T. Sato, R. W. Graves, P. G. Somerville, *Bull. Seismol. Soc. Am.* **89**, 579 (1999).
8. S. Kinoshita, H. Fujiwara, T. Mikoshiba, T. Hoshino, *J. Phys. Earth* **40**, 99 (1992).
9. K. Koketsu and S. Higashi, *Bull. Seismol. Soc. Am.* **82**, 2328 (1992).
10. H. Suzuki, *Rep. Nat. Res. Inst. Earth Sci. Disast. Prev.* **56**, 77 (1996).
11. J. H. Woodhouse, *Geophys. J. R. Astron. Soc.* **37**, 461 (1974).
12. V. Červený, I. A. Molotkov, I. Pšenčík, *Ray Method in Seismology* (Charles University, Prague, 1977).

13. We thank the Japan Meteorological Agency; the National Research Institute of Earth Science and Disaster Prevention; the Tokyo Metropolitan Government; the Tokyo Fire Department; the Prefecture Governments of Kanagawa, Saitama and Chiba; and the City Governments of Yokohama, Kawasaki, and Sagamihara for providing strong ground motion records. Supported by Monbusho (grant 10490010).

11 January 2000; accepted 20 March 2000

Evolutionary Exploitation of Design Options by the First Animals with Hard Skeletons

R. D. K. Thomas,* Rebecca M. Shearman,† Graham W. Stewart‡

The set of viable design elements available for animals to use in building skeletons has been fully exploited. Analysis of animal skeletons in relation to the multivariate, theoretical "Skeleton Space" has shown that a large proportion of these options are used in each phylum. Here, we show that structural elements deployed in the skeletons of Burgess Shale animals (Middle Cambrian) incorporate 146 of 182 character pairs defined in this morphospace. Within 15 million years of the appearance of crown groups of phyla with substantial hard parts, at least 80 percent of skeletal design elements recognized among living and extinct marine metazoans were exploited.

Fundamentally different strategies for constructing hard skeletons emerged in the evolution of each animal subkingdom (*1*) now recognized on the basis of ribosomal RNA sequences (*2, 3*) and patterns of early embryonic development (*4*). The Ecdysozoa (*2*) consist largely of animals that molt their skeletons periodically, as the name implies. The Lophotrochozoa (*3, 5*) include protostomes with external skeletons that typically grow by accretion. Internal skeletons that can be remodeled, especially in more derived taxa, are characteristic of the Deuterostomia. The Skeleton Space (*6, 7*) is a theoretical morphospace that provides a framework, independent of time and the characters of any given group of organisms (*8*), in which to assess rates and patterns of exploitation of morphospace by these animals. We use it here to analyze the initial, early Cambrian emergence of hard parts that complemented, and to varying degrees replaced, hydrostatic skeletons of metazoans that evolved to larger sizes.

A span of 40 million years (*9*) embraces the appearance of the first small, simple shells that may have been secreted by metazoans and the subsequent exuberant diversity of Chengjiang (*10*) and the Burgess Shale (*11–14*). This is not so short a time for an evolutionary "explosion." However, the proliferation of animals with the well-differentiated hard parts characteristic of specific metazoan phyla was largely restricted to the last 15 million years of this interval (*15*). We address three issues: How rapidly were the opportunities of skeletal morphospace taken up in this evolutionary radiation? What patterns of change over time are expressed in the skeletal designs of these early metazoans? To what extent were changes in the genetic basis of pattern formation, the expansion of taxonomic diversity, and the exploitation of design options concurrent?

Department of Geosciences, Franklin & Marshall College, Lancaster, PA 17604, USA.

*To whom correspondence should be addressed. E-mail: r_thomas@acad.fandm.edu

†Present address: Department of Organismal Biology and Anatomy, University of Chicago, 1027 East 57 Street, Chicago, IL 60637, USA.

‡Present address: Rose Center for Earth and Space, American Museum of Natural History, 200 Central Park West, New York, NY 10024, USA.

Our theoretical morphospace is based on seven general properties of animal skeletons or their components. Each has two, three, or four broadly defined states, illustrated here schematically and by examples drawn from animals of the Burgess Shale, of early Middle Cambrian age, in British Columbia (Fig. 1):

1) A skeleton may be internal, as in the elephant, or external, as in the lobster.

2) The skeleton may be composed of rigid material like vertebrate bone, or it may be flexible like the notochord of the lancet.

3) A skeleton may consist of one element, as in most snails; two, like the bivalved shells of animals evolved independently in several different classes and phyla; or multiple elements, as in crinoids and crabs.

4) In shape, the parts of skeletons are essentially rods, plates, or solids. Rods define and support spatial frameworks, like the scaffolding formed by sponge spicules, or they are used as levers, like vertebrate limb bones. Interlocking plates, like those of tortoise shells and sand dollars, enclose space. A cone is a folded plate; we set these apart because they are so widely used as external skeletons. Three-dimensional solids are typically machine parts, like ankle bones, vertebrae, and teeth.

5) Growth of a skeleton that must function continuously as it develops can be accomplished by accretion, as in molluscan shells; by molting and replacement; by the addition of units to a modular structure, as in colonial organisms; or by the sort of remodeling that makes ball-and-socket joints possible in mammals.

6) Most skeletal parts grow in place, where they function, but some are prefabricated and then moved into working position, such as shark's teeth.

7) Multiple components are integrated in